Dust Devils: characteristics of the forward motion from a Saharan survey

Authors:

Gabriele Franzese[1], Simone Silvestro[1,2], David A. Vaz[3], Ciprian Ionut Popa[1], Fabio Cozzolino[1], Francesca Esposito[1], Giuseppe Mongelluzzo[1,4], Carmen Porto[1], Alan Cosimo Ruggeri[1].

[1] *Osservatorio Astronomico di Capodimonte, Istituto Nazionale di Astrofisica, Napoli, Italy*

[2] *SETI Institute, Mountain View, CA, USA*

[3] *Centre for Earth and Space Research of the University of Coimbra, Coimbra, Portugal.*

[4] *Dipartimento di Ingegneria Industriale, Università degli studi di Napoli "Federico II"*

Key words: Dust Devils; Boundary Layer Wind; Micrometeorology; Earth; Mars.

Abstract

Dust devils have been proposed as a tool to investigate martian near-ground wind conditions. However, further studies are needed in order to fully understand how background atmospheric conditions affect dust devil forward motion. One of the main issues is related to the lack of synchronous acquisition of the dust devils forward speed and ambient wind measurements.

This work aims to present an effective methodology to retrieve the dust devil translational velocity using the horizontal wind time series acquired by a single stationary anemometer, and utilize this method to deeply investigate its relation with the ambient velocity.

For this purpose, we first tested the reliability of our method using the data acquired during an intensive week-long dust devil survey, during which we deployed a meteorological station coupled with a camera in a Sahara desert site. After confirming the technique by comparing the results with the ones obtained with the camera, we applied the method to a meteorological data set of 338 dust devil events we acquired in a previous Saharan campaign. We studied the characteristics of the forward velocity, observing how it closely matches the ambient wind regime, with ∼70% of the events lying in a range of 20° and 1 m/s from the ambient velocity measured at 4.5 m. Our results indicate how the vortex forward speed follows a vertical profile similar to the boundary layer wind, confirming the effectiveness of the dust devils monitoring for the study of the surface winds.

1. Introduction

Dust devils are frequent in the terrestrial deserts, but also on Mars, where they are widespread over the surface with a peak in activity around the local summer (Edgett and Malin, 2000; Malin and Edgett, 2001; Greeley et al., 2004; Cantor et al., 2006; Stanzel et al., 2008; Reiss, 2018). They are convective vortices powered by the solar radiation. These vortices are more efficient in dust lifting than standard non-rotating boundary layer winds thanks also to the so called ΔP-effect due to their low pressure core (Greeley et al., 2003; Neakrase et al., 2016; Bila et al., 2019). Despite being studied for more than 150 years (Baddeley 1860; Bagnold 1941; Ives 1947; Grant 1949), we are still not able to fully understand and model the properties of these convective vortexes. Dust devils remain an active topic of research in particular on Mars, where they give a substantial contribution to the planetary dust budget (∼50%) (Kahre et al., 2006; Whelley and Greeley, 2008; Guzewich et al., 2015). In particular, they represent the principal source of the martian haze outside the dust storm seasons (Neubauer, 1966; Thomas and Gierasch, 1985; Murphy and Nelly, 2002; Fisher et al., 2005). The vortex rotatory motion is superposed on its forward translation, the latter mostly led by the drag of the background wind. Hence, as a first approximation, dust devil forward motion is representative of the local wind regime (Balme et al., 2012).

Rodríguez and Bech 2020 remarked the importance on Earth of satellite monitoring for the superficial convective phenomena, in particular for the low-densely populated areas that often lack of in situ meteorological records. Moreover, the capacity to couple dust devil observations with synchronous monitoring of environmental meteorological parameters is crucial for the understanding of the vortex physics (see e.g. Lorenz et al., 2018). The lack of in situ meteorological wind regime and dust devil observations is clearly worse on Mars. Direct measurements of the martian wind regime are restricted to the few areas visited by the missions equipped with meteorological sensors, such as: the Viking landers (Chamberlain et al. 1976), and partially the Pathfinder, Phoenix and Insight landers (Gunnlaugsson et al. 2008; Holstein-Rathlou et al. 2010; Banfield et al. 2019) and the Curiosity rover

(Newman et al. 2017). Data availability is further limited by the anomalies incurred by the wind speed and direction sensors, such as those with Pathfinder and Curiosity (see Martínez et al. 2017 for a review of the subject). However, active dust devils and their tracks can rather be observed from orbit with an almost global coverage, thus they have been proposed as a tool to obtain indications on the boundary layer wind regime. However, this possibility still needs further investigation in order to understand its uncertainty limits. The data acquired from orbit, compared to the in-situ measurements, are generally biased toward larger and taller dust devils, with faster rotating and travelling speed (e.g. see Fenton et al. 2016 for a review of the subject). This could lead to a bias in the extrapolations on the ambient wind regime. Moreover, the study of the relationship between the dust devils motion and the ambient wind is still preliminary. Indeed, given a statistically significant sample, it can exhibit large gradients in both travel speed and direction, with single events that can strongly differ from the average characteristics. In addition, these characteristics can significantly differ from one area of observation to another (Stanzel et al. 2006).

At the time of writing, dust devil forward motion parameters (e.g. the horizontal forward velocity) have been evaluated using time-lapse image sequences of their passage (see Fenton et al. 2016 for a review). One of the main issues that limits the study and comprehension of dust devil physics is the difficulty of resolving the vortex forward motion components and the vortex missing distance from the station using the measurements acquired by a single anemometer (Franzese et al., 2020; Kahanpää et al., 2020). Kahanpää et al., 2020 has analyzed the dust devils recorded in the Curiosity REMS (Rover Environmental Monitoring Station) data, noticing how dust devil missing distance and forward velocity cannot be retrieved independently with their model. Tratt et al. 2003 have pointed out how the ability to measure and account for the dust devil translational motion is essential to unambiguously characterize the dynamics of the vortex. Here we propose a methodology to investigate the vortex translational speed and direction directly by using the acquired horizontal wind time series. The technique is based on the Rankine vortex model and on the simplifying assumption of a uniform rectilinear forward motion. In order to validate this model, we analyzed a survey of

Saharan dust devils comprised of both meteorological and imaging data. We selected a data set of six dust devils visible in more than one image to evaluate their travel velocities and we verified the consistency of our results by comparing the results with the modeled ones. We then applied the method to a large Saharan sample of 338 dust devils acquired in a campaign we performed in 2014, where only the meteorological data were available. We focused on the characteristics of the vortex translational motion, to study how closely the forward velocity mirrors the average wind regime and its vertical profile, and what are the factors that can lead to a deviation from it.

The work is structured as follows:

- section 1 introduces the topic and the previous literature (par. 1.1);
- the methods section (2) is divided in § 2.1, that describes the field campaigns we carried out, and § 2.2 where our model is presented;
- the result section (3) is divided in § 3.1, where the results of the model test with the dust devils image sequences are presented, and § 3.2 that presents the results of the analysis of the 2014 data;
- the discussion and the conclusion are addressed in sections 4 and 5.

1.1 Previous Works

Early studies of dust devil motion noted that dust devils tend to move with speed and direction comparable to the background ambient winds (Flower 1936; Ives, 1947; Williams, 1948; Sinclair, 1969; Croizer, 1970; Maxworthy, 1973). Snow and McClelland 1990 reported a survey where they estimated the travel speed for hundreds of events, comparing it with the ambient wind. They observed how the vortices advance on average at 4 m/s, consistently slower than the background wind measured at 10 m of height. However, these studies give only a qualitative estimation of the relation between dust devil forward motion and ambient wind regime. Balme et al. 2012 have been the first to perform a quantitative study of this topic. Contrary to Snow and McClelland 1990, they have observed how, for their sample, the dust devils travel consistently ~10% faster than the wind speed

at 10 m height. Hence, it is still not clear to what extent the dust devils forward speed follows the vertical profile of the surface layer wind described by the so-called law of the wall (von Karman 1930; Bagnold 1941).

On Mars, the first dust devil columns have been observed by the Viking orbiters (Thomas and Gierasch, 1985). Cantor et al., 2006 were able to measure the travel speed of one dust devils using two Viking Orbiter images of Syria/Sinai plains, taken with a delay of 5 sec. However, crucial progress on the ability to consistently retrieve the forward motion parameters from the orbital images has arrived with the time-sequence imaging of the surface provided by the High Resolution Stereo Camera (HRSC) onboard of the ESA Mars Express mission (Neukum et al., 2004; Jaumann et al. 2007). The three HRSC stereo channels cover the same surface at different times, allowing the study of the dust devils motion. Stanzel et al. 2006 have been the first to analyze the dust devils forward speed, using images triplets of the HRSC. Using the same technique, Stanzel et al. 2008 have reported 205 events from both martian hemispheres. They compared the observed forward velocities with the wind regime expected from the Martian Climate Database (MCD) (Lewis et al., 1999; Forget et al., 1999; Millour et al. 2008), observing how the vortex directions were on average consistent with the modeled winds. However, they reported cases where dust devil forward directions show a chaotic behavior, like in Terra Cimmeria. Reiss et al. 2011 have compared the Martian Orbital Camera (MOC) and the HRSC images taken of Syria planum with a maximum time delay of 12 hours, to search for the dust devils imaged by both instruments. Using the HRSC images they evaluated an average travel speed of 12 m/s.

The possibility of studying dust devils travel speed has been further improved by NASA Mars Reconnaissance Orbiter (MRO) mission, thanks to the combination of the different instrument on board, as the Compact Reconnaissance Imaging Spectrometer (CRISM) (Murchie et al., 2007), the Context Camera (CTX) (Malin et al., 2007) and the High Resolution Image Science Experiment (HiRISE) (McEwen et al., 2007). For example, the different swaths of the HiRISE camera cover the same surface area with a time interval of ~0.1 m/s. This method has been used by Choi and Dundas

2011 and Reiss et al. 2014b. However, due to the short time delay, such a method introduces a strong uncertainty and the resulting forward speeds are only indicative, especially for the events moving slower than ~ 5 m/s. Reiss et al. 2014a introduced a more reliable method, using the simultaneous images taken by the CTX and HiRISE cameras, in combination with the CRISM ones, that are acquired with a delay of ± 1 min. They found 26 CRISM images containing at least one dust devil visible also in the HiRISE or CTX image, for a total of 47 identified dust devils. Comparing the results with the MCD, they concluded that the dust devils travel speeds can be used as a rough proxy of the near-surface winds, taking however into account that in some cases the vortex forward motion is completely unmatched by the simulations. On average, the results from orbit are in agreement with the statement of Balme et al. 2012, indicating how the dust devils translational direction closely mirrors the ambient wind direction, and how the speed is representative of the wind at several meters from the surface.

Dust devil travel speeds have also been studied in situ, mostly using data acquired by missions which were not equipped with meteorological sensors. Greeley et al. 2006 used the image sequences acquired by the cameras of the NASA Mars Exploration Rover Spirit (Squyres et al., 2003) to identify a total of 533 dust devils occurred in Gusev crater during the first dust devil season monitored by the rover. They have evaluated the forward speed for 349 dust devils using sequential images of the same event. They observed, on average, vortices moving slower than the ones reported from orbital measurements, finding a good agreement with the near ground wind speed predicted by the Mars Regional Atmospheric Modeling System (MRAMS) (Rafkin et al., 2001; Rafkin and Michaels, 2003). Greeley et al. 2010 extended the work of Greeley et al. 2006, applying the same technique to all three dust devil seasons monitored by Spirit, identifying more than 700 events and evaluating the travel speed for ~500 of them.

As we mentioned above, one of the greater discrepancies between the dust devil populations observed from orbit and from landed instrumentation is that the latter travel significantly slower. The results from the surface seem to indicate how the dust devils forward speed is representative of the wind

speed at few meters of height, while the orbit results point to higher quotes, in some cases comparable with the height of the Planet Boundary Layer (PBL).

2. Methods

2.1 Equipment and sites

We performed a series of field campaigns in the Sahara desert, in different areas of the Tafilalt region (Morocco), aimed to monitor the local dust lifting events with a fully equipped meteorological station. The campaigns have been carried as part of the development process of the DREAMS station (Dust Characterization, Risk Assessment, and Environment Analyser on the Martian Surface) (Esposito et al. 2018) and the MicroMED (Micro Martian Environmental Dust systematic analyser) instrument (Mongelluzzo et al. 2019, Mongelluzzo et al. 2020; Cozzolino et al., 2020), that are part of the scientific payload of the ESA/Roscosmos ExoMARS missions to Mars. In this work we have focused on the wind data acquired in two Saharan field campaigns performed in 2014 and 2017.

During the 2014 mission we deployed a meteorological station mounted on two separated masts (for a full review of the mission and instrumentation see Esposito et al. 2016 and Aguirre et al. 2017). Here, we study the horizontal wind data acquired by a Campbell Scientific CSAT3 anemometer, mounted at 4.5 m height with a sampling rate of 20 Hz.

During the 2017 campaign we monitored the wind speed and direction using three 2d anemometers (Gill WindSonic) placed at 0.7 m, 2.0 m and 3.35 m, using a sample rate of 0.5 Hz (see Fig. 1; for a full review of the mission and instrumentation see Franzese et al. 2020). We coupled the 2017 meteorological station with a camera, in order to capture the images of passing dust lifting events. The imaging sample rate was synchronized with the anemometers. The measuring site is characterized by a flat dust surface that lasts in the direction where the camera is pointing for more than one hundred meters, except for the small pebbles hill located at ~30 m from the station (Fig.1). The data of both campaigns as the software used for the analysis are available upon request.

Fig. 1 The meteorological station deployed during the 2017 field campaign. The first small pebbles hill visible behind the station is located at ~ 30 m from it. The second line of higher hills is located at ~ 100 m.

2.2 Wind signature model

2.2.1 Definition of the problem

The motion of the vortex is the composition of a translational and a rotational component.

Following the Rankine vortex model, the dependence of the rotational speed (v_r) on the distance from the vortex center (d) can be described as (see e.g. Rankine 1901):

$$v_r(d) = \begin{cases} V_r \dfrac{R}{d} & if\ d > R \quad (1a) \\ V_r \dfrac{d}{R} & if\ d < R \quad (1b) \end{cases}$$

where R is its radius. Namely a region bounded by $d=R$ in solid body rotation, surrounded by a region where the velocity field is irrotational. The surface identified by d = R is usually referred to as vortex wall.

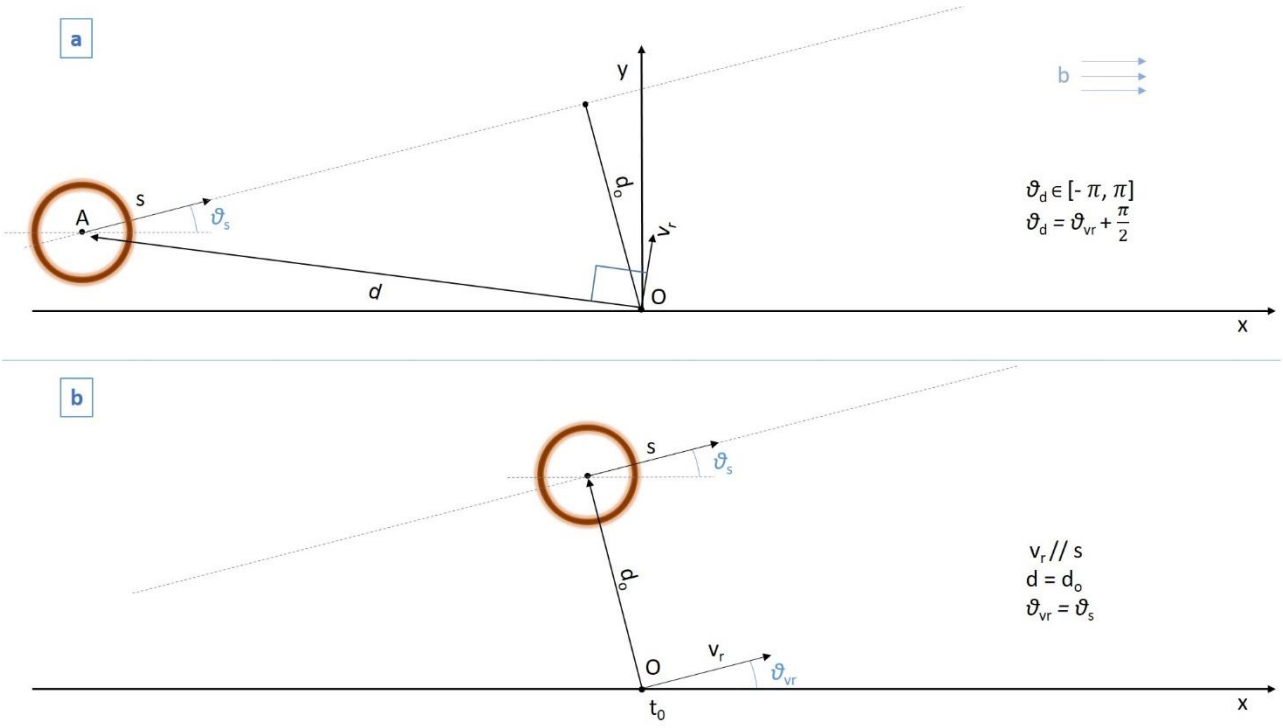

Fig. 2 *Schematization of the passage of a dust devil concordantly rotating. The chosen reference frame has the x axes parallel to the environmental wind speed b and is centered on our station. The vortex translates at speed s. In a) it is still far from the station; in b) the vortex at instant $t=t_0$ reaches the minimum distance from the instruments. Being $\boldsymbol{v_r // s}$ in $d=d_o$, we have $\boldsymbol{\vartheta_{vr} = \vartheta_s}$ (for the discordant rotation: $\boldsymbol{\vartheta_{vr} = \vartheta_s + \pi}$).*

The vortices are embedded in the environmental wind, for this reason their translational speeds (***s***) match on average the background wind velocity (***b***). Indeed, most of the dust devils show a rectilinear translational path. However more complex trajectories have been observed (Reiss et al. 2016).

A dust devil is a dynamic phenomenon, constantly evolving in order to reach equilibrium with air packs and terrains it crosses. However, the typical duration of the acquired meteorological signatures is of the order of tens of seconds. For such a short time, the approximation of steady state is reasonable. We hence suppose that vortex radius, translational speed, rotating speed, core pressure drop and the environmental wind regime remain constant for the entire duration of the encounter. Moreover, we assume that the vortex translates straight and approximatively as a solid body, i.e. the

vortex outer region is moving forward with the same speed $\boldsymbol{s}$ of the core. Lastly, we consider only events that does not transit directly over the instruments.

Fig. 2 shows the reference frame that we use for the study of the dust devils encounters. The frame is centered on the meteorological station, and for simplicity we chose the x axis to be directed parallel to the ambient wind $\boldsymbol{b}$. We indicate the direction of the generic vector $\boldsymbol{v}$ relative to the x axis as θ_v and its components along and perpendicular to $\boldsymbol{b}$, as $v_{//}$ and $v_{\perp}$.

We relaxed the usual approximation $\boldsymbol{s} \equiv \boldsymbol{b}$, supposing for the translational speed a generic direction θ_s. In other words, we assume that the vortex forward motion, in addition to its speed $s_{//}$ along the direction of the background wind, may have a perpendicular component $s_{\perp}$. During its path the vortex will eventually reach a point of maximum approach to the station at time $t=t_o$. We call this minimum distance impact parameter d_o (see Fig. 2 b).

During the dust devil encounters, we monitor the total wind speed $\boldsymbol{V_T}$, that is given by the sum of the background wind regime $\boldsymbol{b}$, plus the speed of the vortex relative to this background. We call $\boldsymbol{w}$ this relative speed, it represents the composition of the vortex translational ($\boldsymbol{s}$) and the rotational speed ($\boldsymbol{v_r}$), minus the wind background:

$$\boldsymbol{w}(t) \equiv \boldsymbol{V_T}(t) - \boldsymbol{b} = \boldsymbol{s} + \boldsymbol{v_r}(t) - \boldsymbol{b} \qquad \textbf{(2)}$$

Dividing w in components:

$$\begin{aligned} w_{\perp} &= s \sin\theta_s + v_r \sin\theta_{v_r} \\ w_{||} &= s \cos\theta_s + v_r \cos\theta_{v_r} - b \end{aligned} \qquad \textbf{(3)}$$

For the orthogonal components holds: $V_{T\perp} = w_{\perp}$, because for definition $b_{\perp}= 0$. Thus:

$$V_T \sin\theta_{V_T} = w \sin\theta_w \qquad \textbf{(4)}$$

From the wind measurement $\boldsymbol{V_T}$ is not possible to directly separate the three components: the background component $\boldsymbol{b}$, the translational $\boldsymbol{s}$ and rotation $\boldsymbol{v_r}$. Here, we propose an operative procedure to isolate them.

2.2.2 Evaluation of the motion components

The easiest wind component to evaluate is the environmental regime ***b***. Indeed, we can simply average the measured V_T on a representative time windows centered on the dust devil encounter. We used an interval of 20 minutes. Knowing *b*, we can evaluate the relative speed *w* at each instant using the definition (eq. (2))).

To reduce the number of variables we evaluated the various parameters at the point of maximum approach $d=d_o$, where θ_{v_r} and θ_s are univocally related. Indeed, for concordant rotation $\theta_{v_r} = \theta_s$ (see Fig. 2 b), while for the discordant case $\theta_{v_r} = \theta_s + \pi$. From here on, we will assume the concordant case, however, the procedure is perfectly consistent and lead to the same results also for the opposite rotation.

The measured wind speed V_T reaches its maximum in the point of maximum approach (d_o). The peak of the measured speed V_T is one of the features that allow to recognize the passage of the event, hence d_o is always clearly recognizable in a dust devil encounter (see Franzese et al. 2018). Thus, the measure of $V_T(d_o)$, $w(d_o)$ and $\theta_{V_T}(d_o)$ is straightforward. The direction $\theta_w(d_o)$ can be retrieved using eq. (4).

Evaluating eq. (3) in d_o we have:

$$\begin{aligned} w \sin\theta_w &= (s + v_r)\sin\theta_s \\ w\ \cos\theta_w &= (s + v_r)\cos\theta_s - b \end{aligned} \qquad \textbf{(5)}$$

Hence, we can evaluate the direction θ_s:

$$\operatorname{tg}\theta_s = \frac{w \sin\theta_w}{w\ \cos\theta_w + b} \qquad \textbf{(6)}$$

We approximate the vortex motion as rectilinear and uniform, thus along a direction θ_s constant for the whole encounter.

Now that we have evaluated the direction θ_s we want to calculate also the speed *s*. In our equation *s* and v_r are always coupled, but while *s* is a constant, the measured v_r depends on the distance. It

increases with $d \rightarrow d_o$, up to a maximum in this point (eq.(1)). Thus, as a first approximation we can suppose in d_o the rotation $v_{r//} \gg s_{//} - b$, obtaining from eq. (2)):

$$|v_r| = \frac{V_T \cos\theta_{V_T} - b}{\cos\theta_s} \quad \textbf{(7)}$$

and eq. (3)):

$$s = \frac{w \sin\theta_w}{\sin\theta_s} - |v_r| \quad \textbf{(8)}$$

The absolute value around v_r is necessary to take into account the two possible sense of rotation of the vortex.

The ability to retrieve the point of maximum approach (d_o) and hence the maximum wind speed is crucial for the success of the described method. This capacity could be limited by the oscillations of the wind level signal and by a low acquisition rate, leading to an increased uncertainty in the results. This factor does not represent an issue for the 2014 data that were acquired with a sample rate of 20 Hz, that assures an exhaustive sampling of the wind signal trend. However, the 2017 data were acquired with a slower sample rate, hence the results of each single anemometer could be inaccurate. For this reason, for the 2017 sample, we decided to evaluate the vortex forward speed using the mean of the three different anemometers results. In this way, we increased the number of samples used to analyze each dust devil, allowing for a more accurate estimation of the translational speed.

2.3 Image processing

As a camera, we used a Go-Pro Hero 3 with a set vertical and horizontal field of view of 94.4 ° and 122.6 °, respectively, and a focal length equivalent f = 17.2 mm.

All the software for the image processing was developed in the Wolfram Mathematica® environment. Firstly, we processed the images to remove the stereographic barrel distortion. We used the following map *T:* $(x_d, y_d) \rightarrow (x_u, y_u)$ between the "distorted" coordinate system Ox_dy_d on the image focal plane and the "undistorted" one Ox_uy_u:

$$T(x_d, y_d) \equiv \frac{r_d}{r_u}(x_d, y_d) \quad \textbf{(9)}$$

The radius r_d and r_u are simply the norm of (x_d , y_d) and (x_u, y_u) and are linked thought the function:

$$r_d \equiv 2\, f\, Tan\left(\frac{\theta}{2}\right) \quad \textbf{(10)}$$

where θ is angle between the vector (r_u, f) and the image optical axis: $\theta = ArcTan\left(\frac{r_u}{f}\right)$.

Fig. 3 shows the result of barrel distortion removal processing.

Fig. 3 One of the acquired images before (top) and after (bottom) the removal of the barrel distortion.

The processed images were then geometrically calibrated using the method described in Franzese et al. 2020 (see paragraph 1.3 therein), in order to retrieve the distance between the passing dust devil and the meteorological station. Fig. 4 shows the reference points and the resulting mapping for the geometric calibration.

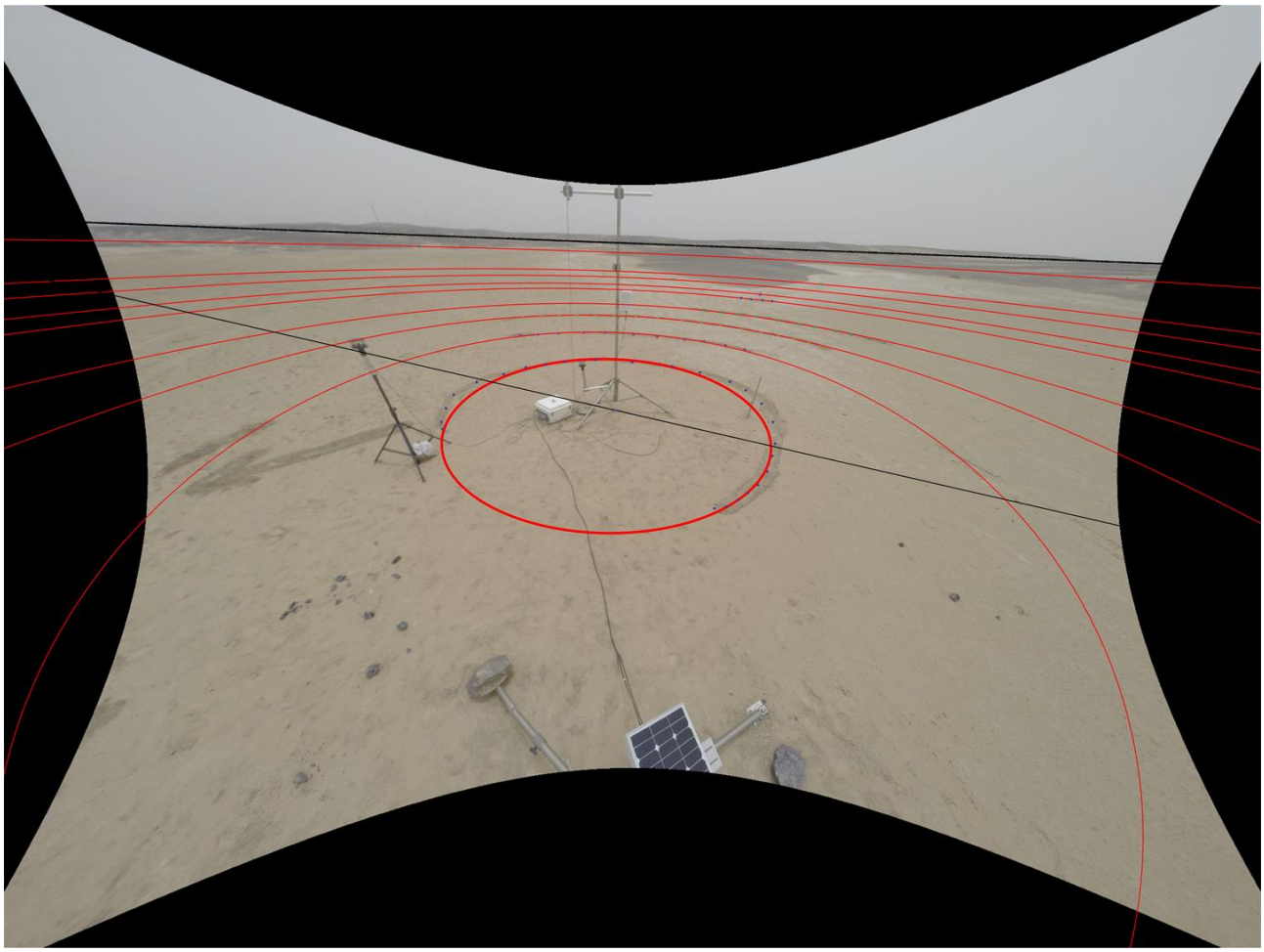

Fig. 4 One of the acquired images with superimposed the geometric calibration map obtained using the marked reference points. The circles indicate a distance of 3, 6, 9, 12, 18, 21, 27, 34 and 114 meters from the meteorological station. The straight lines represent one of the axes passing for the center and the horizon.

We checked the images for dust devils passing inside the field of view of the camera.

The image sequences for each dust devil encounter have been processed subtracting the static component in order to highlight the vortex in motion and derive its position. The result of this process is shown in Fig. 5. By means of the vortex spatial coordinates, transformed using the calibration map, it is possible to reconstruct the dust devils translational path. Then, by knowing the image acquisition rate, it is possible to couple each spatial coordinate with its time, retrieving the forward speed. The

process is similar to the one adopted by Greeley et al. 2006 and Greeley et al. 2010 for the study of the Spirit data. The main uncertainty for this kind of analysis is related to the point distances from the center of the calibrated frame: i.e. the farther the points are from the station, the larger is the uncertainty. For each encounter we decided to fit the time-space coordinates, supposing a simply uniform rectilinear motion, repeating the fit more than once. In the first one we included the first four points closer to the station, then the first eight and so on, increasing the data sample depending on the number of available images in the sequence. We evaluated the forward speed as the mean of the different fit results. In this way, we used the whole range of available distances, but gave more weight to the closer ones. We excluded the images from the analysis, and in some cases the entire encounter, characterized by transits on uneven surfaces, because our mapping requires a flat surface to avoid errors in the results.

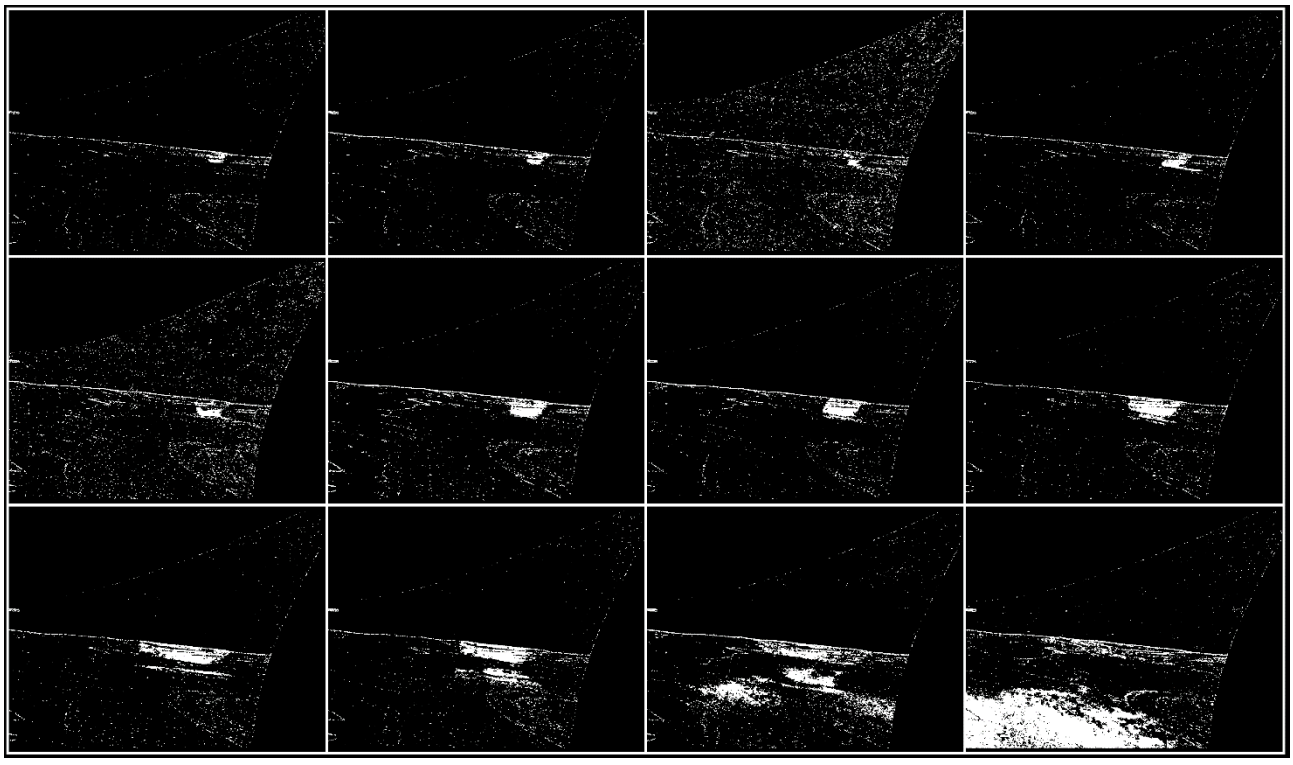

Fig. 5 The image sequence of a dust devils encounter. The sequence advance from left to right, top to bottom. The images are processed subtracting the static component. This technique highlights the vortex silhouette against the surface. The portion that stands out against the sky is not visible here. The conical shape of the vortex is highlighted in white, in the last image is visible a portion of the inner part of dust column base.

3. Results

3.1 Test of the technique

We analyzed the events collected on 23 and 24 July 2017, for a total of six dust devils. The forward wind speed of these events has been evaluated using both the image sequences technique and the meteorological one, in order to verify the reliability of the latter.

Fig. 6 a) shows an example of the spatial coordinates sequence retrieved from the images for one of these encounters. The resulting fit for this event is shown in Fig. 6 b), where the distances sequence is plotted as a function of time.

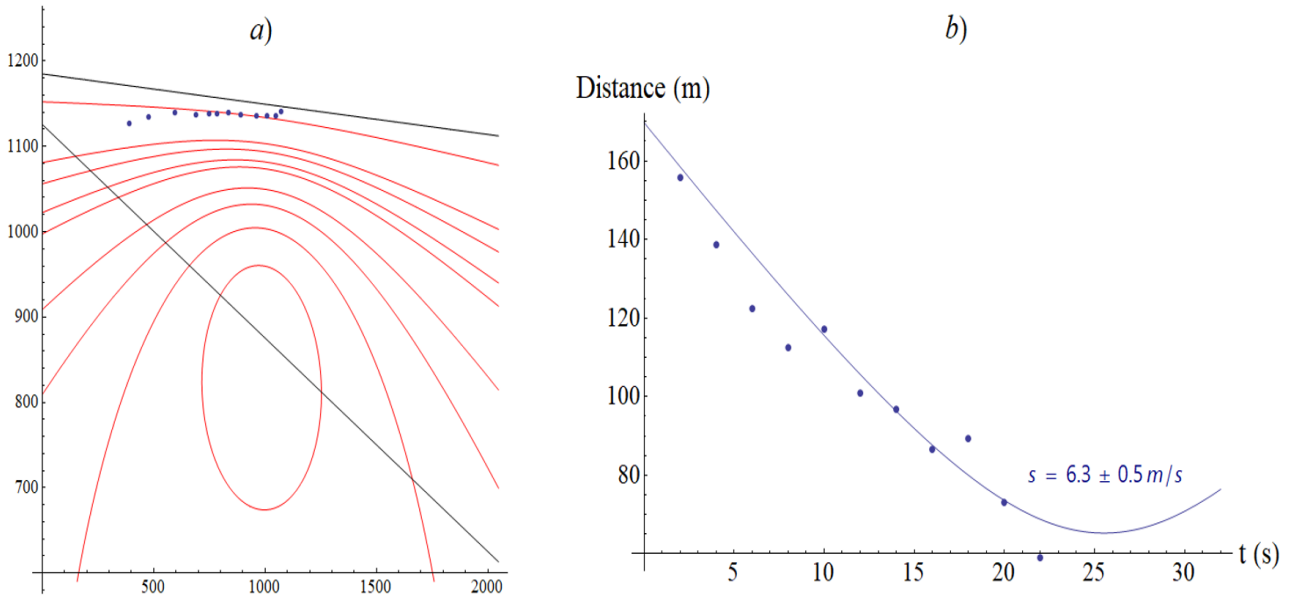

Fig. 6 a) Spatial coordinates of a dust devils moving in one of the image sequences, with the superimposed geometric calibration. The x and y axis are in image pixels. b) The distances sequence of this encounter with the curve resulting from the fitted forward speed.

Fig. 7 shows the acquired wind time series for the same event, where one can easily recognize: a) the speed peak related to the dust devil approaching the station, and b) the change in wind direction due to vortex rotation, that generates an increasing component of the speed perpendicular to the environmental wind ($V_\perp$ in d). As the dust devils pulls away from the station, $V_\perp$ returns to zero.

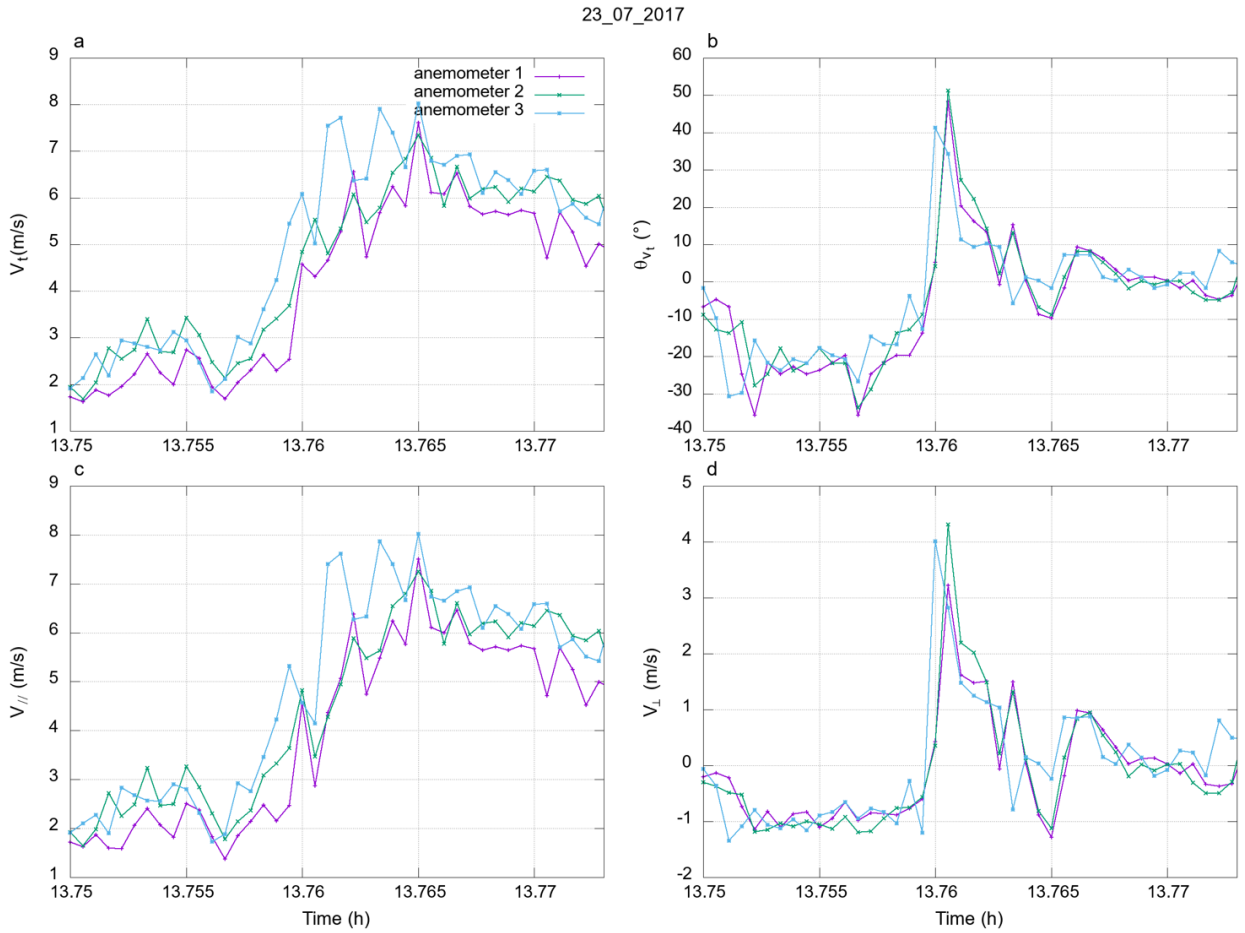

Fig. 7 The wind speed (a) and direction (b) time series for the event depicted in Fig. 6. The speed has been divided in the component parallel (c) and perpendicular (d) to the environmental wind. The anemometers are labeled from below to upwards.

The results for the whole acquired dust devils sample are presented in Table 1 and graphically compared in Fig. 8. For both methods, the uncertainty level is highly variable from one event to another. Here, for consistency purposes, we decided to present all the results rounded at first decimal digit. The two methods give comparable results for each encounter, confirming the reliability of our meteorological analysis technique. We hence proceeded to the analysis of the larger data set acquired in the 2014 field campaign.

S wind	**S images**
4.3 ± 0.5	5.0 ± 0.9
6.7 ± 1.3	6.3 ± 0.5
6.9 ± 0.9	6.7 ± 0.7
5.4 ± 1.1	5.7 ± 1.1
6.5 ± 1.2	6.3 ± 0.2
6.3 ± 1.1	6.7 ± 1.3

Table 1 Results of the dust devils forward wind speed *s* evaluated using the wind time series (s_{wind}) and the image sequences (s_{images}).

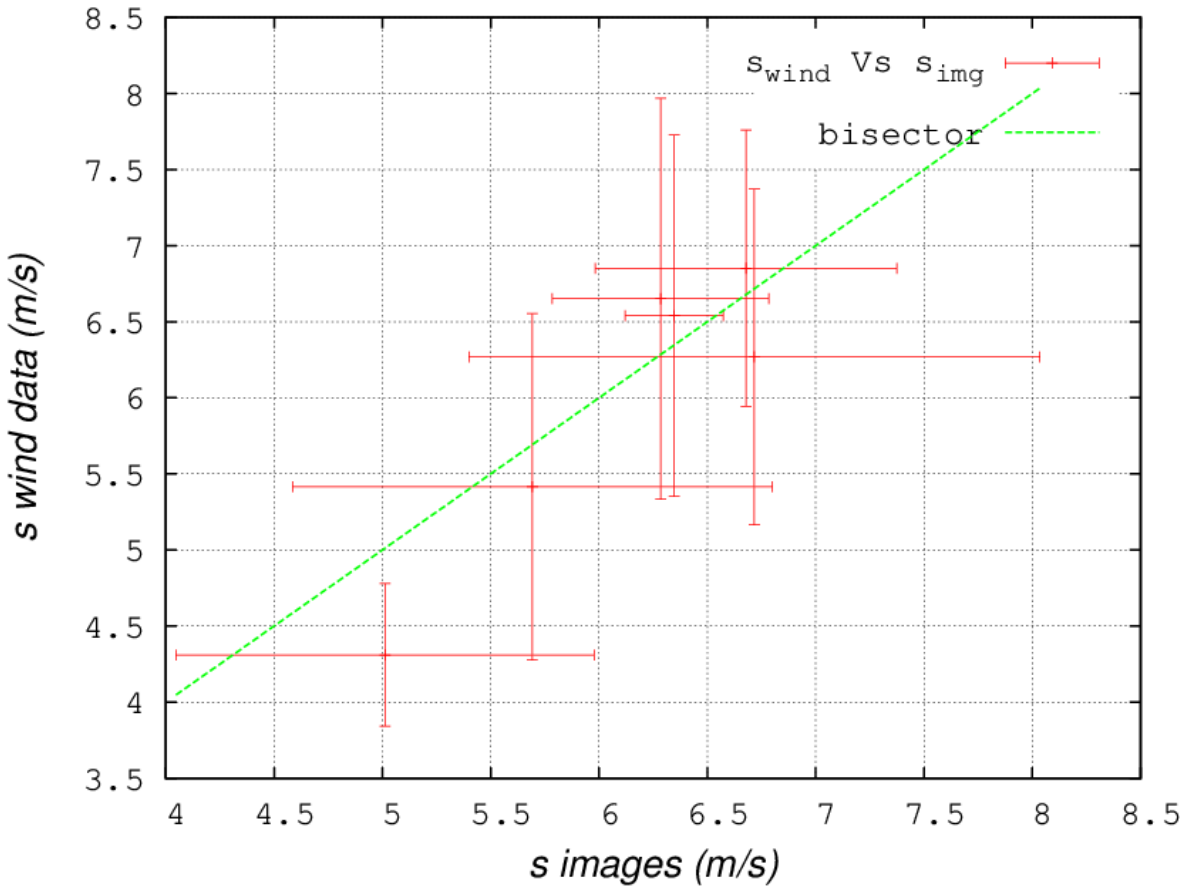

Fig. 8 Comparison of the forward wind speed *s* evaluated using the meteorological method (y-axis) and the image sequences method (x-axis). Note how all the points lie on the bisector within their uncertainties, confirming the compatibility of the two approaches.

3.2 Analysis of the 2014 data

During the Saharan field campaign performed in 2014, we monitored the local dust lifting events from the middle of June to the beginning of September. Here, we focus on the last 53 days of acquisition, when the meteorological station was also equipped with a 3d anemometer. We selected the 3d wind data because of their higher acquisition rate (20 Hz).

We obtained a data set of 338 events, for the description of how the dust devils have been identified in the daily meteorological time series please refer to Franzese et al. 2018. The full data table with the input parameters and the retrieved travel speed and directions can be found in the supplementary materials.

Fig. 9 shows the distribution of dust devils directions ($\Delta\theta_s \equiv \theta_s - \theta_b$ in a) and speeds ($\Delta s \equiv |s\text{-}b|$ in b), with respect to the background wind regime, in terms of the Probability Density Function (PDF). The distribution of $\Delta\theta_s$ can be reasonably described with a gaussian of standard deviation $\sigma\sim20°$, while the trend of Δs can be well approximated with an exponential distribution of type $B\, e^{-B\, x^C}$ properly normalized. Hence, about 68% of the observed vortices advance in a direction that differs less than 20° from the one of the background wind, with this difference overcoming 30° only in 14 % of the cases. On average, we obtained a $|\Delta\theta_s|\sim15°$. Regarding the speed values, we obtain that the probability to find dust devil travelling more than 2 m/s faster than the background wind is only ~17%, while ~70% of the measures lie under the 1 m/s of difference. In median, the dust devils are ~ 9% faster than the *b* evaluated at height 4.5 m.

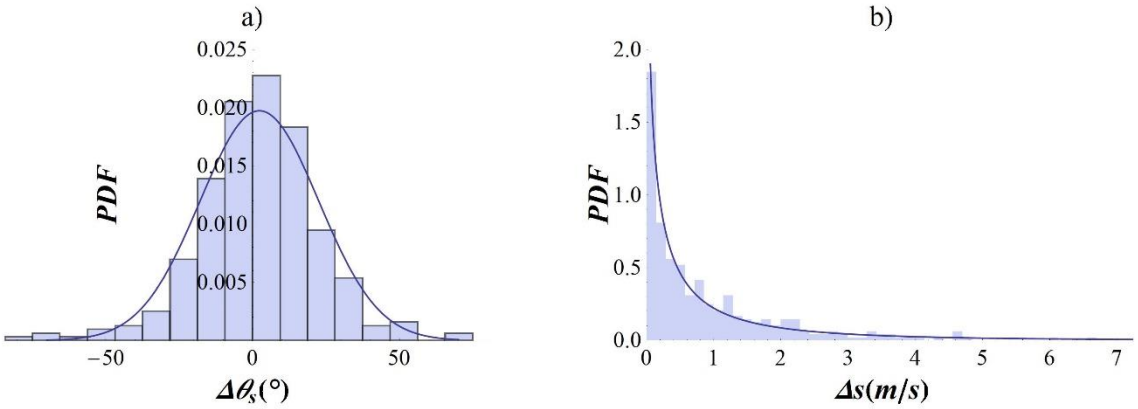

Fig. 9 The probability density function of the difference between the dust devils travel speed and the environmental wind, as direction (a) and speed (b).

As shown in Fig. 10, $\Delta\theta_s$ and Δs clearly correlate: an increase of the relative translational speed Δs corresponds to an increase of the deviation of the trajectory from the background wind direction $\Delta\theta_s$. After an initial steep increment, for higher values of Δs the trend seems to reach a plateau around $\Delta\theta_s$ = 20°, in agreement with what we observed in Fig. 9 a).

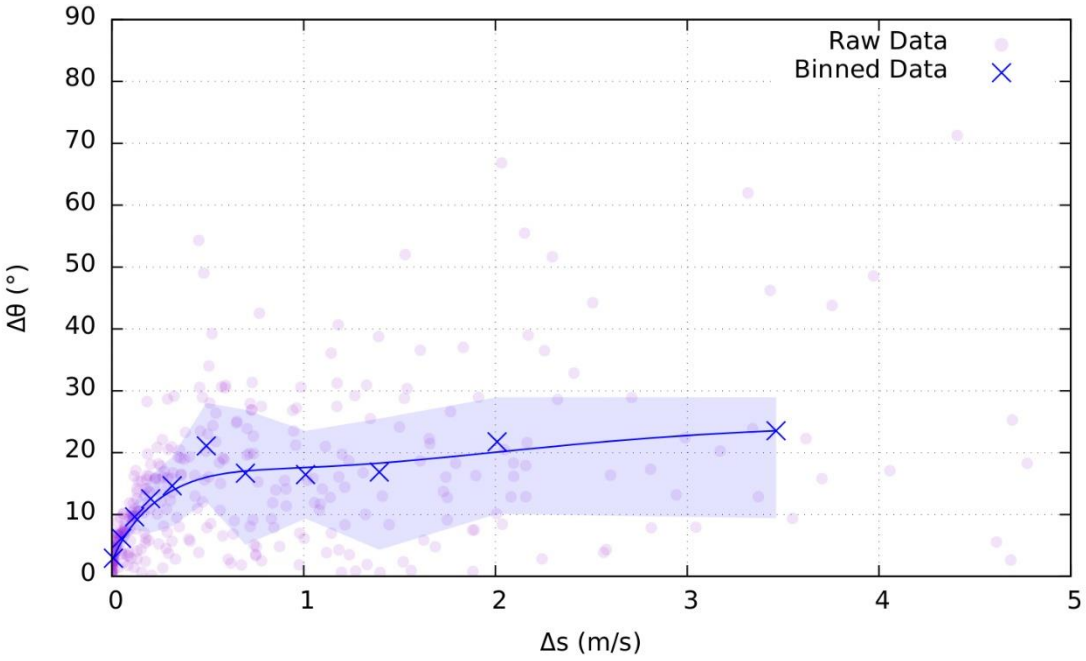

Fig. 10 Relation between the dust devils relative forward speed and direction. In transparency the uncertainty levels are presented in terms of quartiles.

We also studied what are the other parameters that can lead to an increase of the vortices forward path deviation from the environmental wind. Balme et al., 2012 have observed how the daily circular standard deviation (σ_{θ_s}) of the dust devils directions decreases with the increases of the mean environmental wind. In Fig. 11 we compared the data of our 50 active days of measurements (the days where we observed non-zero dust devils activity) with the ones acquired by Balme et al., 2012. The range of variation of σ_{θ_s} is comparable, however in our data we do not observe days characterized by a daily mean of $\boldsymbol{b}$ lower than 3 m/s, hence the initial trend of the Eloy and Eldorado data is not visible.

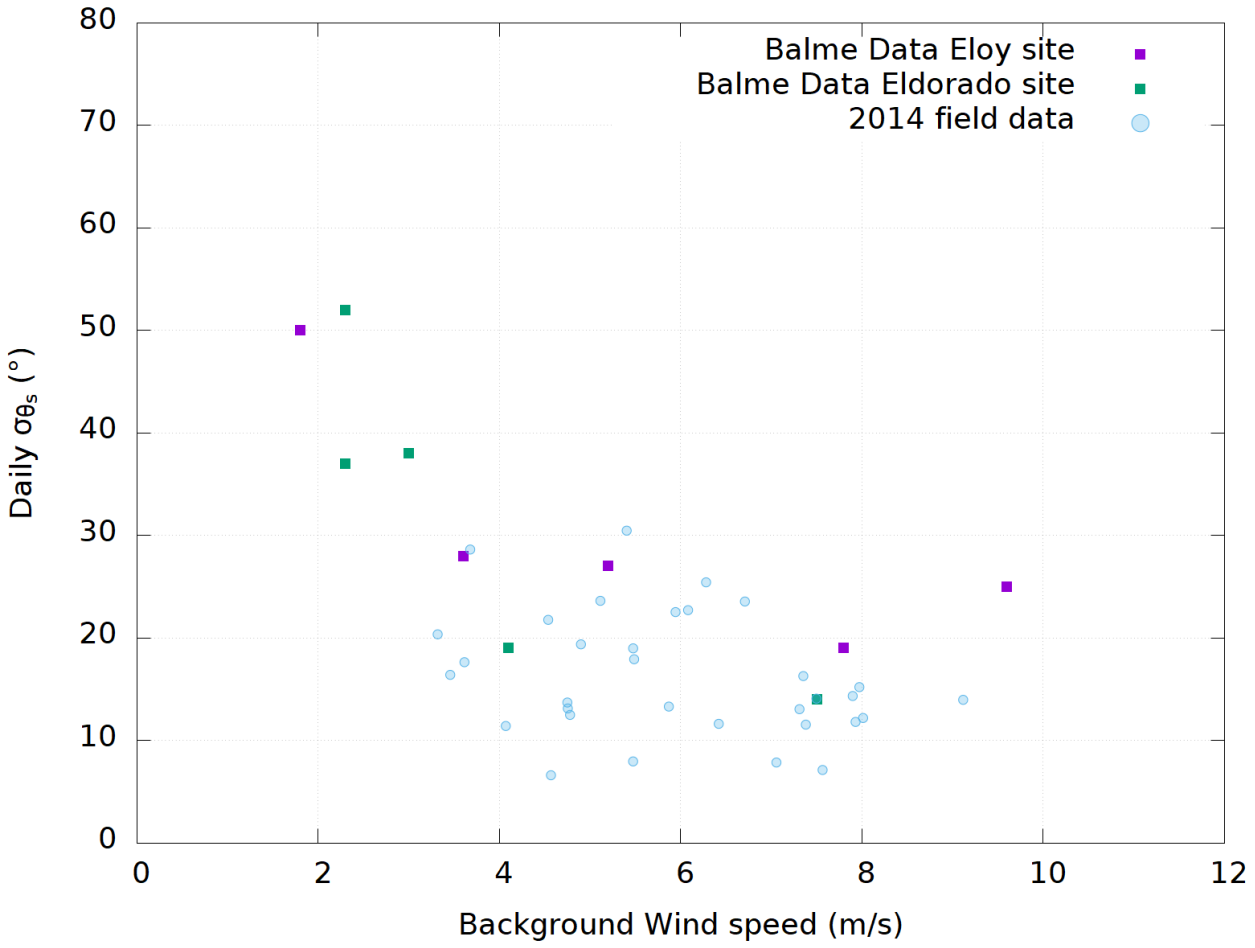

Fig. 11 Deviation of the dust devils forward direction (expressed as circular standard deviation) as a function of the background wind speed. The quantities on both axes are presented in terms of daily mean. The dataset acquired by Balme et al. 2012 is showed as comparison.

Instead using the circular standard deviation of the dust devil directions, we decided to focus on the $\Delta\theta_s$ parameter, namely the angle between the vortex travel direction and the direction of the ambient wind. Indeed, the evaluation of $\Delta\theta_s$ doesn't require to group the data on a daily base, potentially mixing very different wind conditions, but each $\Delta\theta_s$ is representative of the single vortex encountered. As shown in Fig. 12 a), we observed how $\Delta\theta_s$ is strictly related to the environmental wind speed *b*. In this representation is clearer how the deviation of the dust devil directions rapidly decreases with the increase of ***b***, and how the slope of the relation diminishes for values of $b > 4$ m/s, tending toward a flatter behavior. Moreover, we observed how $\Delta\theta_s$ is positively related to the circular standard deviation (σ_{θ_b}) of the ***b*** vector, with an almost flat behavior for $\sigma_{\theta_b} < 60°$ (see Fig. 12 b).

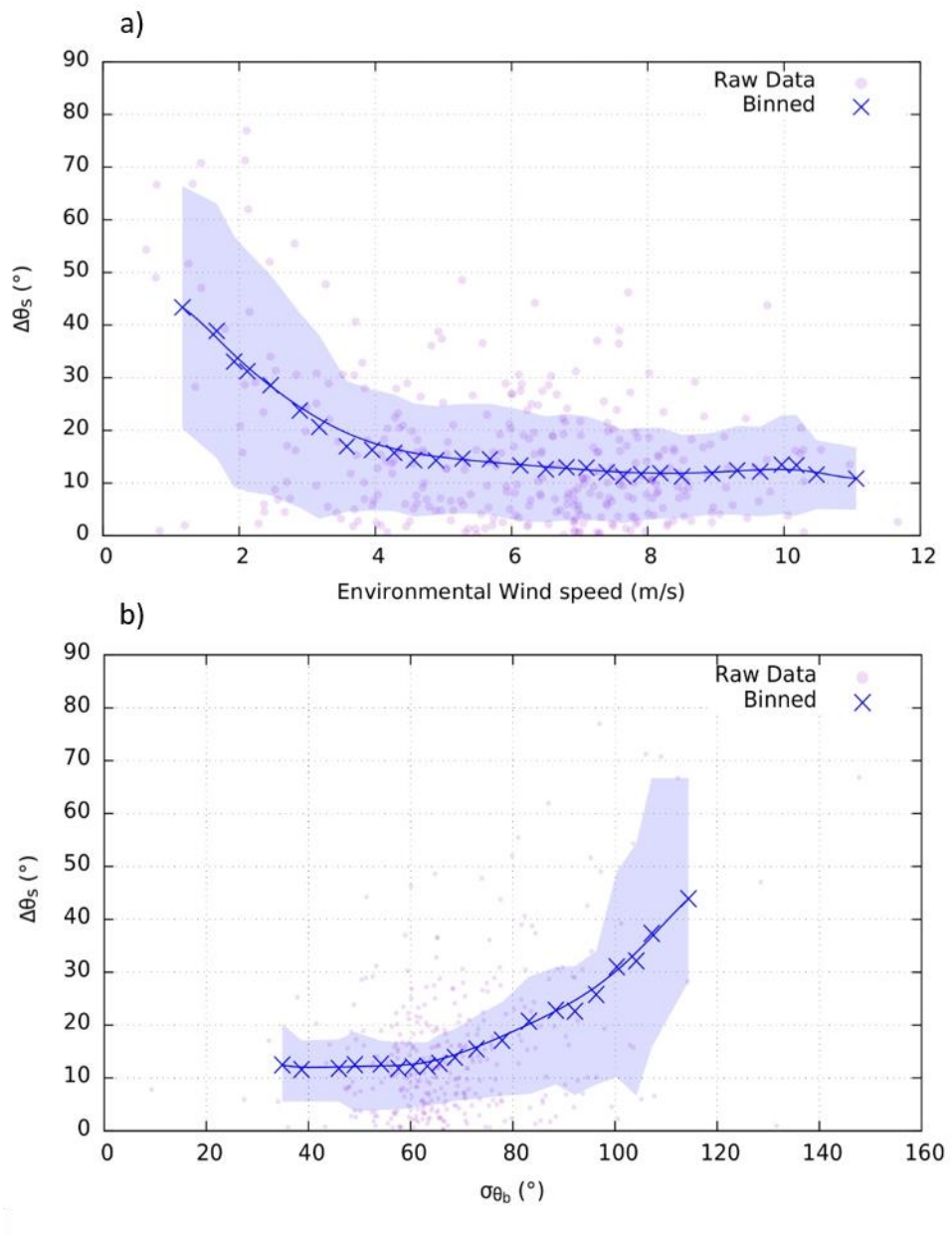

Fig. 12 Relations between the deviation of the dust devil direction ($\Delta\theta_s$) from the mean wind direction and the mean wind speed *b* (in a) and the circular standard deviation (σ_{θ_b}) of the *b* direction (in b).

4. Discussion

4.1 Analysis of the 2014 data set

The general indication that dust devils translate on average in a direction concordant with the environmental wind is commonly supported by the literature. Indeed, also our data show how dust devils consistently travel within 20°-30° of the prevailing wind direction. This value is in agreement

e.g. with the ones of 45° and 30° reported by Sinclair 1969 and Balme et al. 2012, respectively. Instead, the question on the correspondence between the near ground wind speed and the dust devils travel speed, and then on the vertical profile of the latter, is still open. The reported results are indeed contrasting.

An indication that the vertical profile of the vortex forward speed closely mirrors the boundary layer wind vertical shear is given by the tilt that many events exhibit in the wind direction, as reported also on Mars f.e. from Ferri et al., 2003 for the Pathfinder, Stanzel et al. 2008 for the Super Resolution Channel (SRC) and Greeley et al. 2006 for the Spirit images. However, also this indication is not unambiguous, considering that this property is not always recognizable in the terrestrial or martian events.

Balme et al. 2012 has observed how the vortices consistently move between 10 and 20% faster than the ***b*** measured at 10 m. Indeed, they suggested how the travel speed seems representative of the wind regime around 20-30 m of height, with the vortex forward speed being almost constant with the height. These results are qualitatively in agreement with the orbital martian surveys (Stanzel et al., 2006; Stanzel et al. 2008; Reiss et all, 2011; Reiss et al., 2014a) but not with the in situ ones (Greeley et al. 2006; Greeley et al. 2010). Our data are instead characterized by dust devils ∼9% faster than the mean wind at 4.5 m. We can assume, as a first approximation, a simple neutral logarithmic wind profile:

$$u(z) = \frac{u^*}{k} ln\left(\frac{z}{z_o}\right) \quad \textbf{(11)}$$

where u is the wind speed, z the height, u^* the friction velocity and z_o the roughness. Taking into account that using the 3d anemometer measurements we evaluated a z_o ranging between 0.001 and 0.04 m, this translates to a height of 7-8 m above the ground in order to match the dust devils forward speed. This value is lower than to the one indicated by Balme et al. 2012, moreover our data also suggest a different interpretation of this speed discrepancy Δs. Rather than a travel speed representative of the environmental wind speed at higher height, the difference seems related to a

secondary component of the translating motion, perpendicular to the environmental one (the one we referred to as $s_{\perp}$). As we showed in Fig. 9 and Fig. 10, this component is secondary and only leads to a mean deviation of 15° from the environmental wind direction, with the vortices rarely overcoming the 30° of deviation. Lorenz 2016 have shown how the deviation $\Delta\theta_s$ of the data of Balme et al. 2012, averaged on a daily base, can be fitted with a Atan(R/b) model. Where R is interpretable as some kind of "constant random windspeed" superimposed to b, with a best fit of R=2.5 m/s. Following this approach, we tried to fit the deviation $\Delta\theta_s$ reported in Fig. 12 a) with an Atan(R/b) model obtaining a good match with our data for an R=0.8 ± 0.3 m/s. Lorenz 2016 suggests how this component R could be related to the deviation of the vortex motion from the straight line pattern, toward a cycloidal or trochoidal trajectory. However, it is worth to mention how no direct signs of non-straight line patterns are visible in our data set. Hence, we suggest how a secondary motion component ($s_{\perp}$) exists, probably related to the local oscillation of the horizontal wind speed near the vortex formation area, as supported by the positive relation between the deviation $\Delta\theta_s$ from the mean direction and the circular standard deviation σ_{θ_b} of $\boldsymbol{b}$ (see Fig. 12 b).

As we said the conclusions on the nature of Δs of Balme et al. 2012 are in agreement with the results of the martian orbital surveys, but the different interpretation here proposed can help also to resolve the discrepancies with the in situ observation. Stanzel et al. 2006, reporting a sample of 17 dust devils, observed discrepancies between the near ground wind speed modeled with the MCD and the measured dust devils speed. They observed that the 5 events in Thaumasia Planum move significantly faster than the expected wind, while the speed of the ones in Amazonis Planitia is more in agreement with the MCD. Considering that the vortices in Thaumasia Planum are on average much taller than the ones of Amazonis Planitia, they interpreted the result as an indication that the measured speed was representative of the speed at the top of the column and not of the near ground value. This suggests that the dust devil speed has a vertical profile with a significant increase from the bottom to the top. However, they argue that the result is not unambiguous because 2 of the 5 dust devils in Thaumasia Planum, despite being of similar height to the ones of Amazonis Planitia, still travelled

much faster than the expected value. A similar result has been reported by Reiss et al. 2014a, that measured the travel speed for 47 dust devils, observing how it is significantly faster (around a factor 2) than the wind speed at 10 m predicted by the MCD. The dust devils speeds, with a mean value around 20 m/s, are instead in good agreement with the wind speed evaluated at the top of the dust column, thus at an altitude comparable with the PBL height.

The vortex is characterized by a central region in helicoidally raising pattern and an outer region where the air tends to re-fall down. However, the prevailing vertical motion is in the upward direction, tending to raise the slower air layers toward the faster ones and not vice versa. For this reason, we consider unlikely the possibility that the bottom of the column could travel with a speed comparable with the top of the boundary layer.

Regarding the data acquired from the surface, Greeley et al. 2006 and Greeley et al., 2010 have reported a median dust devils forward speed around 2 m/s during the three seasons monitored by Spirit, that is consistent with the value predicted by MRAMS for the environmental wind at 2 m of height. During the first monitored season, where the faster-moving population was reported, the forward speed overcomes 12 m/s only in three cases. In addition, they observed how this travel speed tends to increase during the morning reaching the maximum around noon, where most of the dust devils moving faster than 2 m/s have been reported, consistently with the increased environmental wind speed expected at that time.

The orbital cameras resolution limits can partially explain the bias toward larger and taller dust devils observed from orbit respect the ones detected from the landed instruments. However, this can't explain the bias toward faster events. Neither the terrestrial or martian data, from orbit and surface, indicates a trend of increasing forward speed for the larger dust devils (Stanzel et al. 2008; Greeley et al. 2010; Balme et al. 2012; Reiss et al. 2014a). Reiss et al. 2011, using the dust sample of 26 dust devils and 2 dust plumes they recognized in HRSC images, even reported how the dust devils with smaller diameters tend to move faster, even if no true relation between travel speed and size was

observable. The same tendency has been reported also by Greeley et al., 2010 for the ~500 dust devils acquired by Spirit in Gusev crater.

Our results support the hypothesis that the forward velocity measured from orbit is relative to the top of the column which can move significantly faster than the base of the dust devil. This means that the vortex forward speed approximates the background wind at each height, mirroring its vertical profile. The small discrepancies in speed and direction are attributable to the fluctuation of the ambient wind velocity in the area of the vortex formation, that lead by inertia to a small secondary component of the translation. Such a deviation rapidly decreases as the prevailing wind increases, in particular above the 4 – 5 m/s wind speed (Fig. 12).

Lastly, we have also to consider that the way the background wind affects the dust devil motion and its stability depends on a combination of factors that cannot be completely addressed in this work. Indeed, the interaction ambient wind - dust devil is heavily affected by the vortex morphology. Further surveys, able to monitor both the environmental and the intrinsic vortex parameters (as its pressure core drop, rotatory and translational velocity, diameters and height), are still required in order to investigate the topic both on Earth and on Mars.

5. Summary and Conclusions

The monitoring of the dust devil forward motion has been proposed in literature as a tool for roughly investigating the near ground wind regime. However, previous measurements report ambiguities and discrepancies that limit the usefulness of this kind of studies. In this paper, we investigated this topic in order to find a solid interpretation compatible with both terrestrial and martian measurements.

We proposed a method to derive the translational speed and direction of the dust devils by monitoring the horizontal wind velocity. The possibility to study the dust devils motion from the wind time series is crucial for the understanding of their physics, allowing a direct comparison with the environmental wind conditions. We tested our technique using the data we acquired in a Sahara Desert campaign, where we monitored the dust devil activity acquiring both the wind speed time series and the image

sequences of vortex passages. Our results confirm that, despite the simplicity of the methodology and its assumptions, with this technique we are able to consistently retrieve the forward motion parameters of the observed events.

Using this method, we deeply analyzed a previous three months long Saharan survey, where we monitored the local dust devil population without the aid of a camera. We evaluated the translational speed and direction for 338 events, comparing the results with the measurements of the local wind regime. Our data not only indicate that the vortices consistently translate along the direction of the prevailing wind, but they also shed light on the open questions regarding the magnitude at different height of this speed. Indeed, we observed how the forward velocity closely matches the one of the near ground wind, indicating how both follow a similar vertical profile. Small deviations from the environmental wind have been observed, relatable to the local fluctuation of the wind regime. The increase of the wind speed and the decrease of its circular standard deviation minimize these deviations.

Our results bearing out the utility of the dust devils as a probe of the environmental wind condition. This is of particular interest in the martian environment, in optics to utilize the remote control of the dust devil activity for investigation the near ground wind regime, thus partly remedying the lacks of in situ meteorological detectors. Moreover, the here proposed technique for evaluation dust devil forward velocities is of special interest in the frame of the next martian missions that will deploy on the surface sensors capable of the meteorological monitoring of the dust lifting events, as the MEDA (Mars Environmental Dynamics Analyzer) suite on board of the NASA Mars 2020 mission or the METEO package on board of the ESA/Roscosmos ExoMars 2022. Our method will allow to fully characterize the dynamics of the observed dust devils, resolving their translational and rotational motion component. The METEO package in particular will work alongside the MicroMED instruments and the other sensors belonging to the Dust Complex, allowing to characterize the dust devils also from an electric and dust load point of view.

Acknowledge

The authors want to thank the Ibn Battuta centre and the EuroPLANET research infrastructure for the support provided. EuroPLANET 2020 RI has received funding from the European Union's Horizon 2020 research and innovation programme under grant agreement No 654208. D. Vaz acknowledge support from CITEUC (project UID/Multi/00611/2020).

References

Aguirre, C., Franzese, G., Esposito, F., Vazquez, L., Caro-Carretero, R., Vilela-Mendes, R., ... & Popa, C. I. (2017). Signal-adapted tomography as a tool for dust devil detection. *Aeolian Research*, *29*, 12-22.

Baddeley, P. F. H. (1860). *Whirlwinds and Dust-storms of India: An Investigation Into the Law of Wind and Revolving Storms at Sea: with an Addendum Containing Practical Hints on Sanitary Measures Required for the European Soldier in India* (Vol. 1). Bell & Daldy.

Banfield, D., Rodriguez-Manfredi, J. A., Russell, C. T., Rowe, K. M., Leneman, D., Lai, H. R., ... & Joy, S. P. (2019). Insight auxiliary payload sensor suite (apss). *Space Science Reviews*, *215*(1), 4.

Bagnold, R. A. (2012). *The physics of blown sand and desert dunes*. Courier Corporation.

Balme, M. R., Pathare, A., Metzger, S. M., Towner, M. C., Lewis, S. R., Spiga, A., ... & Michaels, T. I. (2012). Field measurements of horizontal forward motion velocities of terrestrial dust devils: towards a proxy for ambient winds on Mars and Earth. *Icarus*, *221*(2), 632-645.

Bila, T., Wurm, G., Onyeagusi, F. C., & Teiser, J. (2020). Lifting grains by the transient low pressure in a martian dust devil. *Icarus*, *339*, 113569.

Cantor, B. A., Kanak, K. M., & Edgett, K. S. (2006). Mars Orbiter Camera observations of Martian dust devils and their tracks (September 1997 to January 2006) and evaluation of theoretical vortex models. *Journal of Geophysical Research: Planets*, *111*(E12).

Cozzolino, F., Mennella, V., Ruggeri, A. C., Mongelluzzo, G., Franzese, G., Popa, C. I., ... & Scaccabarozzi, D. (2020). Martian environment chamber: Dust systems injections. *Planetary and Space Science*, 104971.

Crozier, W.D., 1970. Dust devil properties. J. Geophys. Res. 75, 4583–4585.

Edgett, K. S., & Malin, M. C. (2000). New views of Mars eolian activity, materials, and surface properties: Three vignettes from the Mars Global Surveyor Mars Orbiter Camera. *Journal of Geophysical Research: Planets*, *105*(E1), 1623-1650.

Esposito, F., Molinaro, R., Popa, C. I., Molfese, C., Cozzolino, F., Marty, L., ... & Ori, G. G. (2016). The role of the atmospheric electric field in the dust-lifting process. *Geophysical Research Letters*, *43*(10), 5501-5508.

Esposito, F., Debei, S., Bettanini, C., Molfese, C., Rodríguez, I. A., Colombatti, G., ... & Schipani, P. (2018). The DREAMS experiment onboard the Schiaparelli module of the ExoMars 2016 mission: design, performances and expected results. *Space Science Reviews*, *214*(6), 103.

Fenton, L., Reiss, D., Lemmon, M., Marticorena, B., Lewis, S., & Cantor, B. (2016). Orbital observations of dust lofted by daytime convective turbulence. *Space Science Reviews*, *203*(1-4), 89-142.

Ferri, F., Smith, P. H., Lemmon, M., & Renno, N. O. (2003). Dust devils as observed by Mars Pathfinder. *Journal of Geophysical Research: Planets*, *108*(E12).

Fisher, J. A., Richardson, M. I., Newman, C. E., Szwast, M. A., Graf, C., Basu, S., ... & Wilson, R. J. (2005). A survey of Martian dust devil activity using Mars Global Surveyor Mars Orbiter Camera images. *Journal of Geophysical Research: Planets*, *110*(E3).

Flower, W.D., 1936. Sand devils. Lon. Met. Off. Prof. Notes 5, 1–16.

Forget, F. et al., 1999. Improved General Circulation Models of the martian atmosphere from the surface to above 80 km. J. Geophys. Res. 104, 24155–24175.

Franzese, G., Esposito, F., Lorenz, R., Silvestro, S., Popa, C. I., Molinaro, R., ... & Deniskina, N. (2018). Electric properties of dust devils. *Earth and Planetary Science Letters*, *493*, 71-81.

Franzese, G., Della Rocca, V., & Esposito, F. (2020). Resolution of the size/distance degeneracy of the dust devils signals observed with a stationary meteorological station. *Aeolian Research*, *44*, 100594.

Franzese, G., Silvestro, S., Vaz, D., Popa, C., and Esposito, F.: Terrestrial and Martian Dust Devils: study of the translational motion and resolution of the size/distance degeneracy of the meteorological time series, EGU General Assembly 2020, Online, 4–8 May 2020, EGU2020-21323, https://doi.org/10.5194/egusphere-egu2020-21323, 2020

Grant, C. G. (1949). Dust devils in the sub-arctic. *Weather*, *4*, 402-403.

Greeley, R., Balme, M. R., Iversen, J. D., Metzger, S., Mickelson, R., Phoreman, J., & White, B. (2003). Martian dust devils: Laboratory simulations of particle threshold. *Journal of Geophysical Research: Planets*, *108*(E5).

Greeley, R., Whelley, P. L., Arvidson, R. E., Cabrol, N. A., Foley, D. J., Franklin, B. J., ... & Lemmon, M. T. (2006). Active dust devils in Gusev crater, Mars: observations from the Mars exploration rover spirit. Journal of Geophysical Research: Planets, 111(E12).

Greeley, R., Waller, D. A., Cabrol, N. A., Landis, G. A., Lemmon, M. T., Neakrase, L. D., ... & Whelley, P. L. (2010). Gusev Crater, Mars: Observations of three dust devil seasons. Journal of Geophysical Research: Planets, 115(E7).

Guzewich, S. D., Toigo, A. D., Kulowski, L., & Wang, H. (2015). Mars Orbiter Camera climatology of textured dust storms. *Icarus*, *258*, 1-13.

Ives, R. L. (1947). Behavior of dust devils. *Bulletin of the American Meteorological Society*, *28*(4), 168-174.

Jaumann, R., Neukum, G., Behnke, T., Duxbury, T. C., Eichentopf, K., Flohrer, J., ... & Hoffmann, H. (2007). The high-resolution stereo camera (HRSC) experiment on Mars Express: Instrument aspects and experiment conduct from interplanetary cruise through the nominal mission. *Planetary and Space Science*, *55*(7-8), 928-952.

Kahanpää, H., & Viúdez-Moreiras, D. (2020). Modelling Martian dust devils using in-situ wind, pressure, and UV radiation measurements by Mars Science Laboratory. Icarus, 114207.

Kahre, M.A., Murphy, J.R., Haberle, R.M., 2006. Modeling the Martian dust cycle and surface dust reservoirs with the NASA Ames general circulation model. J. Geophys. Res. 111. https://doi.org/10.1029/2005JE002588.

Karman, T. (1930). von: Mechanische Ähnlichkeit und Turbulenz, Nachr. Ges. Wiss. Göttingen, Math.-phys. Kl.(1930) 58–76'. *Proc. 3. Int. Cong. Appl. Mech*, 322-346.

Lewis, S. R., M. Collins, P. L. Read, F. Forget, F. Hourdin, R. Fournier, C. Hourdin, O. Talagrand, and J. Huot (1999), A climate database for Mars, J. Geophys. Res., 104(E10), 24,177– 24,194.

Lorenz, R.D., 2016. Heuristic estimation of dust devil vortex parameters and trajectories from single-station meteorological data: application to insight at Mars. Icarus271, 326–337.

Lorenz, R. D., Jackson, B. K., & Lanagan, P. D. (2018). A timelapse camera dataset and Markov model of dust devil activity at Eldorado playa, Nevada, USA. Aeolian research, 33, 33-43.

Malin, M. C., & Edgett, K. S. (2001). Mars global surveyor Mars orbiter camera: interplanetary cruise through primary mission. *Journal of Geophysical Research: Planets*, *106*(E10), 23429-23570.

Malin, M.C. et al., 2007. Context Camera Investigation on board the Mars Reconnaissance Orbiter. J. Geophys. Res. 112, E05S04. http://dx.doi.org/10.1029/2006JE002808.

Martínez, G.M., Newman, C.N., De Vicente-Retortillo, A. *et al.* The Modern Near-Surface Martian Climate: A Review of In-situ Meteorological Data from Viking to Curiosity. *Space Sci Rev* **212,** 295–338 (2017). https://doi.org/10.1007/s11214-017-0360-x

Maxworthy, T. (1973), A vorticity source for large scale dust devils and other comments on naturally occurring columnar vortices, J. Atmos. Sci., 30, 1717–1722.

McEwen, A.S. et al., 2007. Mars Reconnaissance Orbiter's High Resolution Imaging Science Experiment (HiRISE). J. Geophys. Res. 112, E05S02. http://dx.doi.org/10.1029/2005JE002605.

Millour, E. et al., 2008. The latest (version 4.3) Mars Climate Database. In: Third International Workshop on the Mars Atmosphere: Modeling and Observations, held November 10–13, 2008 in Williamsburg, Virginia. LPI Contribution No. 1447. Abstract #9029.

Mongelluzzo, G., Esposito, F., Cozzolino, F., Franzese, G., Ruggeri, A. C., Porto, C., ... & Saggin, B. (2019). Design and CFD Analysis of the Fluid Dynamic Sampling System of the "MicroMED" Optical Particle Counter. *Sensors*, *19*(22), 5037.

Mongelluzzo, G., Esposito, F., Cozzolino, F., Molfese, C., Silvestro, S., Franzese, G., ... & Scaccabarozzi, D. (2019). CFD analysis and optimization of the sensor "MicroMED" for the ExoMars 2020 mission. *Measurement*, *147*, 106824.

Murphy, J. R., & Nelli, S. (2002). Mars Pathfinder convective vortices: Frequency of occurrence. *Geophysical research letters*, *29*(23).

Murchie, S. et al., 2007. Compact Reconnaissance Imaging Spectrometer for Mars (CRISM) on Mars Reconnaissance Orbiter (MRO). J. Geophys. Res. 112, E05S03. http://dx.doi.org/10.1029/2006JE002682.

Neakrase, L. D. V., Balme, M. R., Esposito, F., Kelling, T., Klose, M., Kok, J. F., ... & Wurm, G. (2016). Particle lifting processes in dust devils. *Space Science Reviews*, *203*(1-4), 347-376.

Neubauer, F. M. (1966). Thermal convection in the Martian atmosphere. *Journal of Geophysical Research*, *71*(10), 2419-2426.

Neukum, G., & Jaumann, R. (2004, August). HRSC: The high resolution stereo camera of Mars Express. In *Mars Express: The Scientific Payload* (Vol. 1240, pp. 17-35).

Newman, C. E., Gómez-Elvira, J., Marin, M., Navarro, S., Torres, J., Richardson, M. I., ... & Vasavada, A. R. (2017). Winds measured by the Rover Environmental Monitoring Station (REMS) during the Mars Science Laboratory (MSL) rover's Bagnold Dunes Campaign and comparison with numerical modeling using MarsWRF. *Icarus*, *291*, 203-231.

Rafkin, S. C. R., and T. I. Michaels (2003), Meteorological predictions for 2003 Mars Exploration Rover high-priority landing sites, J. Geophys. Res., 108(E12), 8091, doi:10.1029/2002JE002027.

Rafkin, S. C. R., R. M. Haberle, and T. I. Michaels (2001), The Mars Regional Atmospheric Modeling System: Model description and selected simulations, Icarus, 151, 228– 256.

Rankine, W.J.M., 1901. A Manual of Applied Mechanics. C. Griffin and Co., Limited, London, UK.

Reiss, D., Zanetti, M., & Neukum, G. (2011). Multitemporal observations of identical active dust devils on Mars with the High Resolution Stereo Camera (HRSC) and Mars Orbiter Camera (MOC). *Icarus*, *215*(1), 358-369.

Reiss, D., Spiga, A., & Erkeling, G. (2014a). The horizontal motion of dust devils on Mars derived from CRISM and CTX/HiRISE observations. *Icarus*, *227*, 8-20.

D. Reiss, N.M. Hoekzema, O.J. Stenzel, Dust deflation by dust devils on Mars derived from optical depth measurements using the shadow method in HiRISE images. Planet. Space Sci. **93–94**, 54–64 (2014b). doi:10.1016/j.pss.2014.01.016

Reiss, D., Fenton, L., Neakrase, L., Zimmerman, M., Statella, T., Whelley, P., ... & Balme, M. (2016). Dust devil tracks. *Space Science Reviews*, *203*(1-4), 143-181.

Reiss, D. (2018). Dust Devils: Stirring Up the Martian Surface. In *Dynamic Mars* (pp. 295-316). Elsevier.

Rodríguez, O., & Bech, J. (2020). Reanalysing strong-convective wind damage paths using high-resolution aerial images. Natural Hazards, 104(1), 1021-1038.

Sinclair, P. C. (1969). General characteristics of dust devils. *Journal of Applied Meteorology*, *8*(1), 32-45.

Snow, J.T., McClelland, T.M., 1990. Dust devils at white-sands-missile-range, New-Mexico.1. Temporal and spatial distributions. J. Geophys. Res. 95, 13707–13721.

Stanzel, C., Pätzold, M., Greeley, R., Hauber, E., & Neukum, G. (2006). Dust devils on Mars observed by the high resolution stereo camera. *Geophysical research letters*, *33*(11).

Stanzel, C., Pätzold, M., Williams, D. A., Whelley, P. L., Greeley, R., Neukum, G., & HRSC Co-Investigator Team. (2008). Dust devil speeds, directions of motion and general characteristics observed by the Mars Express High Resolution Stereo Camera. *Icarus*, *197*(1), 39-51.

Thomas, P., & Gierasch, P. J. (1985). Dust devils on Mars. *Science*, *230*(4722), 175-177.

Wolfram Research, Inc., Mathematica, Champaign, Illinois - https://www.wolfram.com/mathematica

Whelley, P. L., & Greeley, R. (2008). The distribution of dust devil activity on Mars. *Journal of Geophysical Research: Planets*, *113*(E7).